Trajectory Optimization of Levitated Particles in Mid-air Ultrasonic Standing Wave Levitators

Tatsuki Fushimi, Asier Marzo, Thomas L. Hill, Bruce W. Drinkwater
Department of Mechanical Engineering, University of Bristol, Bristol, BS8 1TR, United Kingdom
Email: t.fuishimi@bristol.ac.uk

***Abstract*—Ultrasonic standing wave levitators have a broad range of potential applications as a non-contact transportation method in pharmaceutical, chemical, or biological procedures. In these devices, the particle is held in mid-air and moved to the target position, either by mechanically translating the levitator or by refocusing the standing wave with a phased-array. However, most acoustic levitators operate in open-loop mode and do not have feedback on the position of the particle. Without a control system, the path that the levitated particle follows differs significantly from the desired path. Tracking in three dimensions millimeter-sized particles in mid-air at the required frame rates is technically challenging and costly. In response, we explore offline optimization of the trajectory as a solution. The aim of this optimization is to increase the accuracy with which the desired path is followed by the levitated particle, benefitting contactless transportation and manipulation applications. This method could also be applied to display technologies in which a travelling particle outlines different shapes to convey information.**

I. Introduction

Ultrasonic standing wave levitators are devices that utilize the acoustic radiation force to levitate or manipulate particles. They have a broad range of applications as non-contact transportation methods in pharmaceutical, chemical and biological applications. An emerging application of mid-air acoustic levitation is the creation of visual displays in which the particles represent information [1] such as 3D trajectories [2]. In 'JOLED', a screen made of levitated dielectric particles can be flipped individually between binary colors using an electric field [3]. More recently, Uno et al. proposed 'Luciola', a semi-spherical particle embedded with an LED and a coil that was levitated and lit up via wireless powering [4].

In these displays, the particle is held in mid-air and moved to the target position by refocusing the standing wave with a phased-array, the particle serves as a voxel (i. e. 3D equivalent to a pixel in a 2D display). However, as noted by Prisbrey & Raeymaekers [5], the path that the levitated particle follows differs from the desired path. Stable levitation of a particle may be difficult due to irregularities in its shape or the existence of other particles inside the levitator. However, even for a relatively simple case with one spherical particle, it is still non-trivial to follow the desired path. For example, if a particle was set to follow a trajectory as shown in Fig. 1 a), the resultant path of the particle is not identical to the target, as shown in Fig. 1 b).

One potential solution is to use closed-loop control. The implementation of an appropriate closed-loop controller for the system could be expected to reduce the error between target and actual particle position. However, it is technically challenging and costly to track a levitated particle of millimeter-scale size at the required frame rate (>1000 FPS). Thus, we explore offline optimization of the trajectory as a solution, using experimental results to correct for deviations in particle trajectory. More accurate particle trajectories will benefit contactless transportation and manipulation applications as well as increase the understanding of the particle behavior inside mid-air acoustic levitators.

II. Method

The acoustic levitator used to create Fig. 1 is made of two opposed planar arrays. In this case, each array contains 30 ultrasonic transducers (Murata MA40S4S, $f = 40\,\mathrm{kHz}$) arranged as shown in Fig. 2 and separated by $0.080\,\mathrm{m}$.

The transducer signals were generated by an FPGA board (ALTERA CoreEp4CE6) in which 60 independent square waves with a phase resolution of $\phi = \frac{2\pi}{128}$ were generated and amplified to 18 V with MOFSET drivers (TC4427a) and an external DC power supply (RS Pro IPS 303DD) [6].

A. Experimental Setup

In order to identify the cause of the deviation in the trajectory of the levitated particles, a camera (FLIR PointGrey Chameleon 3, with a SV-5014H lens) was directed at the

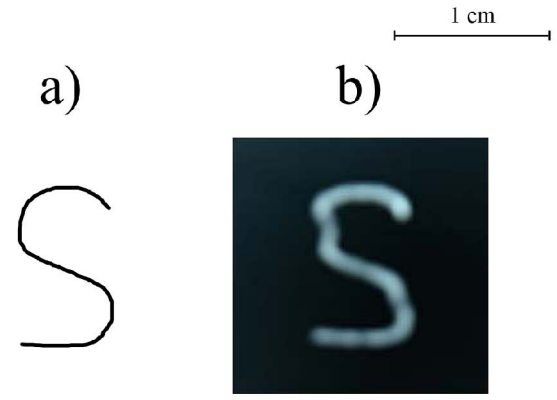

Fig. 1. Particle following trajectory. a) Target trajectory. b) Resultant trajectory.

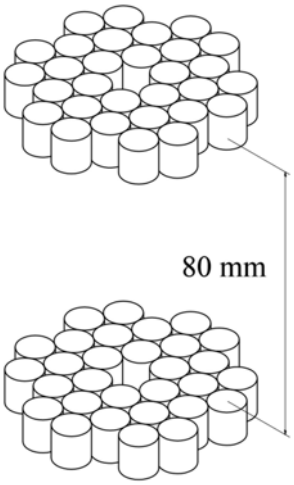

Fig. 2. Transducer positions in the phase-array.

levitator, and an LED light source with a diffuser illuminated from the opposite side, as shown in Fig. 3. The camera records the silhouette generated by the light source, and the particle position is identified by a circle Hough transform implemented in the MATLAB image analysis package. The camera was calibrated using a CMM-stylus (Renishaw A-5000-7806) to find the pixel-to-meter conversion ($4.5 \times 10^{-5}\,\mathrm{m\,pix^{-1}}$) and the datum point in acoustic levitator. The camera setup was checked for lens distortion using a checkerboard, the lens distortion was minimal (i.e. mean reprojection error of 0.28 pixels).

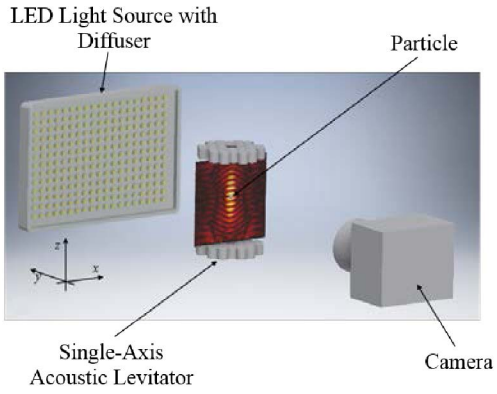

Fig. 3. Experimental setup. At the back, there is an LED light source with a diffuser which generates a silhouette. At the centre, we placed the double-sided planar acoustic levitator made of 60 transducers. At the front, a camera records the particle position.

An expanded polystyrene (EPS) particle was levitated at the central node of the acoustic levitator. The particle is held statically at a series of positions from a grid in the x-z plane. At each new position the equilibrium point of the particle was recorded after settling for 2 seconds. The search space was set to $-0.010 \leq x \leq 0.010$ and $0.030 \leq z \leq 0.050\,\mathrm{m}$ and the focal point was moved with a grid spacing of $0.5\,\mathrm{mm}$. The experiment was conducted in a chamber (width = 4.3 m, height = 2.4 m, length = 2.4 m) on a passive vibration isolation table (Thorlabs PFH90150-8) to minimize external disturbances such as air currents and vibration. Each experiment was repeated three times and the average was taken.

B. Simulation of Particle Equilibrium Point

To identify if the deviation in the path is inherently caused by the pressure field generated by the transducer array, the equivalent results were obtained in simulation by calculating the acoustic radiation force generated by the acoustic levitator. The pressure field generated by the setup was calculated using:

$$p_{in} = \sum_{n=1}^{60} \frac{P_0 D_f(\theta)}{d_n} \mathrm{e}^{\mathrm{j}(\phi_{focal,n} + k d_n)} \tag{1}$$

where $P_0 = 3.38$ Pa when the transducer is driven at 18 V, $k = \frac{2\pi f}{c_0}$ is the wavenumber, $d_n = |\boldsymbol{x_{t,n}} - \boldsymbol{x}|$. $\boldsymbol{x_{t,n}} = (x_{t,n}, y_{t,n}, z_{t,n})$ is the transducer position, $\boldsymbol{x} = (x, y, z)$ is position from a datum point, and f and c_0 are the frequency of the transducers and speed of sound, respectively. $D_f(\theta) = |\frac{2J_1(\nu)}{\nu}|$ is the far-field directivity function for a piston source where J_1 is the Bessel function of the first kind of order 1, $\nu = ka\sin(\theta)$ where $a = 0.0045$ m, and θ is the angle between the transducer normal and the target position $\boldsymbol{x}$. $\phi_{focal,n}$ is the phase-delay applied to each transducer and it is calculated by

$$\phi_{focal,n} = -\frac{2\pi f_0}{c_0}\Big(|\boldsymbol{x_{t,n}} - \boldsymbol{x_f}| - |\boldsymbol{x_f}|\Big) + \phi_{t,n} \tag{2}$$

where $\boldsymbol{x_f} = (x_f, y_f, z_f)$ is the focal point of the acoustic levitator. $\phi_{t,n}$ is the phase shift needed to create an anti-node at the focal point, i.e. $\phi_t = 0$ for the lower phased array and $\phi_t = \pi$ for the upper phased array. Assuming that the particle ($r = 0.78\,\mathrm{mm}$, $m = 0.079\,\mathrm{mg}$, roundness = 0.938) is small in comparison to the wavelength ($\lambda = 8.6\,\mathrm{mm}$), the acoustic radiation force is calculated using Gor'kov's potential [7] [8]:

$$F^{rad} = -\nabla U^{rad} \tag{3}$$

$$U^{rad} = \frac{4\pi}{3} r^3 \Big[\frac{f_1 \kappa_0 \langle p_{in}^2 \rangle}{2} - \frac{3 f_2 \rho_0 \langle v_{in}^2 \rangle}{4}\Big] \tag{4}$$

where $f_1 = 1 - \frac{\kappa_p}{\kappa_0}$, $f_2 = \frac{2(\tilde{\rho}-1)}{2\tilde{\rho}+1}$, and $\tilde{\rho} = \frac{\rho_p}{\rho_0}$. ρ is density, $\kappa = \frac{1}{\rho c}$ is compressiblity, p_{in} and v_{in} are incident pressure and velocity fields, respectively. Subscript 0 represents the property of fluid medium and p represents particle. The equilibrium point of a particle in simulation is determined by balancing the acoustic radiation force and the gravity force ($F_{grav} = mg$).

Fig. 4 shows an example of the acoustic radiation force when the focal point was set to $\boldsymbol{x_f} = (0, 0, 0.040)$ m and the predicted equilibrium point of particle in such field.

C. Distortion in the Equilibrium Point Field

The numerically-predicted equilibrium position of the particle is as shown in Fig. 5. The position of the equilibrium point is close to the focal point and the field is ordered with an

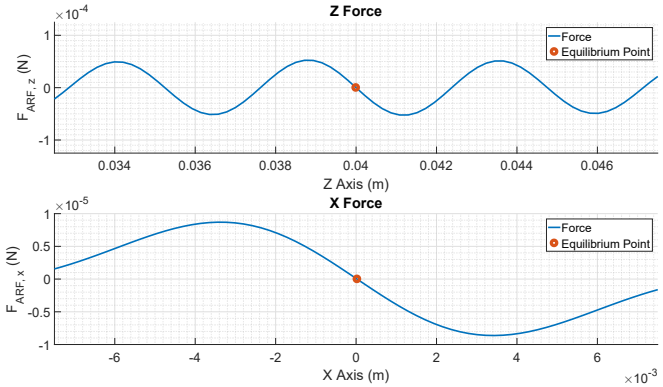

Fig. 4. Acoustic radiation force inside the acoustic field.

RMS value of $0.11\,\text{mm}$ and $0.013\,\text{mm}$ between focal point and equilibrium point in x and z, respectively. As the focal point reaches the sides of acoustic levitator, the equilibrium points shift towards the center of the levitator. This is caused by the directivity of the transducer, as its ability to focus decreases towards the edge of the transducer array.

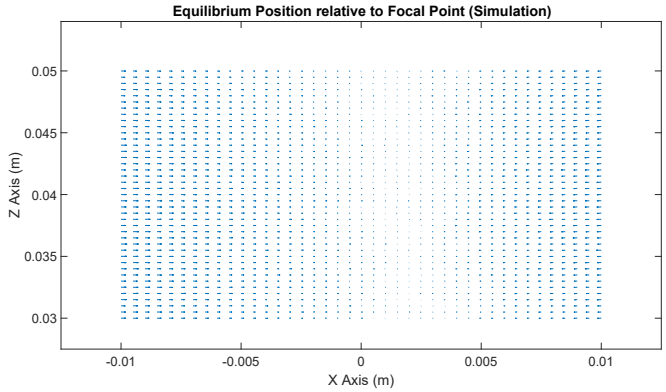

Fig. 5. Position of the equilibrium point relative to the focal point in simulation. The length of quiver is scaled to 1, and shows the error between the particle equilibrium position and the focal point.

On the other hand, the experimentally obtained equilibrium points are distorted as shown in Fig. 6. The deviation of the equilibrium points is more significant than predicted by the numerical simulation and the RMS value between focal point and equilibrium point increases to $0.57\,\text{mm}$ and $0.83\,\text{mm}$ in x and z, respectively. It can be seen that both the direction and magnitude of the experimentally measured deviation varies across the field.

Some deviation in the field may be associated with systematic errors in the calibration datum; the equilibrium points in Fig. 6 are the average position of three separate scans, thus the source of disturbance in field is not external (e. g. air current). The problem observed in Fig. 1 is caused by the distortion of the equilibrium point field, optimization is essential to improve the trajectory. Prisbrey & Raeymaekers recently reported a similar problem and suggested the possibility of scattering from nearby surfaces, non-spherical particles, and

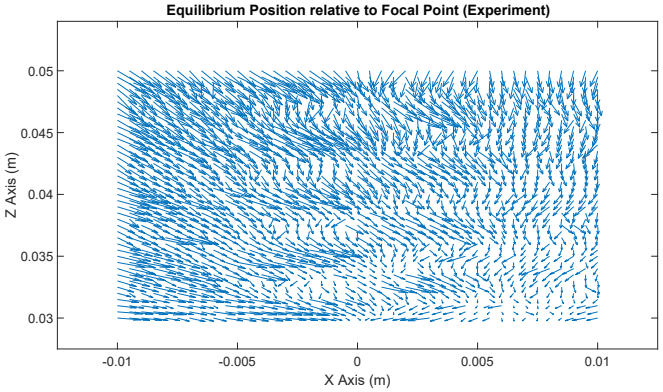

Fig. 6. Position of equilibrium points relative to the focal points in experiment. The length of quiver is scaled to 1, and represents the error between the equilibrium position and the focal point.

imperfections in geometry of transducer array as the source of deviation [5].

As the deviation is caused by unmodeled effects, trajectory optimization using simulations was not feasible. Thus, an experimental approach using the distorted field in Fig. 6 was developed to achieve increased trajectory accuracy in 2D. A correction algorithm is used to find a new set of focal points which achieves the target position at each stage of the trajectory, and the focal points were found by optimizing the function:

$$\min |\boldsymbol{x_T} - \boldsymbol{x_e}| \tag{5}$$

where $\boldsymbol{x_T} = (x_T, z_T)$ is the target position and $\boldsymbol{x_e} = (x_e, z_e) = F(\boldsymbol{x_f})$ is the equilibrium position. Equilibrium points are functions of the focal points, $\boldsymbol{x_f} = (x_f, z_f)$. Using the focal points as the initial guess, the equilibrium points for the given focal points were interpolated (spline) from experimental data, and the optimization function was evaluated for each set of focal points. The correction algorithm used gradient descent to find the suitable set of focal points where its equilibrium points are close to the target particle position, the process was repeated for each step of the trajectory.

III. Results and Discussions

In order to test the effectiveness of the optimization process, a particle was set to follow a circular trajectory, as shown in Fig. 7, the equilibrium points for each step of the trajectory were recorded after settling for 2 seconds. Without any correction, the particle position is offset both in the horizontal (x) and vertical (z) directions and the trajectory is not circular. The RMS between target position and particle position is as shown in Fig. 7 b) and c), and it is 0.51 and $0.79\,\text{mm}$ in x and z, respectively. Alternatively, the maximum pattern error of the path (E_{pat}, mean distance between the user specified and experimentally obtained particle locations, normalized by the wavelength of the field $\lambda = 8.6\,\text{mm}$ as defined in [5]) is $E_{pat} = 17.3\,\%$. The blue dots in Fig. 7 show the particle position after the application of the correction algorithm, which has significantly improved. The RMS value for x and

z are 0.11 and 0.030 mm, respectively and the maximum $E_{pat} = 3.4\,\%$. The correction algorithm has reduced the RMS error by 79.0 % and 96.3 % in x and z, respectively or 80.4 % for maximum E_{pat}.

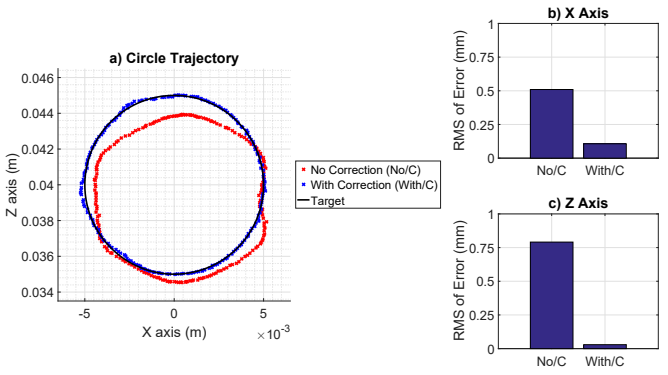

Fig. 7. Quantitative measurements of the effectiveness of the correction algorithm. a) Comparison of the circle trajectory with and without correction. b) RMS error of the path in the x axis. c) RMS error of the path in the z axis.

The correction of the equilibrium points remains effective as long as the focal point movement is slow ($\approx 1\,\text{cm s}^{-1}$). A camera (NIKON D610) was set up similarly to Fig. 3 and the trajectories in the shape of the letters, 'I','E', 'U' and 'S' were sent to the levitator, as shown in Fig. 8 a). The exposure time was set to 4 seconds, thereby the particle outlined the trajectory during the recording. The particle trajectory for the letter shapes without correction is as shown in Fig. 8 b), and the trajectory after the application of the correction algorithm is as shown in Fig. 8 c). It is evident that the correction algorithm has qualitatively improved the trajectory of the particle, demonstrating the applicability of the technique in current display applications where a particle is used as a voxel.

IV. Conclusion and Future Work

In conclusion, the correction algorithm has optimized and improved the trajectory of the particle path in a dynamic acoustic levitator, and demonstrated the applicability in current display applications using acoustic levitation. The implementation in this paper is 2D, however, it can be expanded to 3D by acquiring the 3D position of the particles using additional cameras. Moreover, the correction algorithm may be applied for the case where the particle is not spherical or where multiple particles exist.

Whilst the algorithm is effective for a particle travelling at a slow velocity, the inertia of the particle starts to dominate as the particle is driven at a faster velocity. Previous work [9] has demonstrated the complexity of the particle's dynamic behaviour with a small perturbation in a standing wave levitator. The combined dynamics, together with unmodelled effects described in this paper highlights the challenges and complexity of optimizing the particle trajectory for higher velocities.

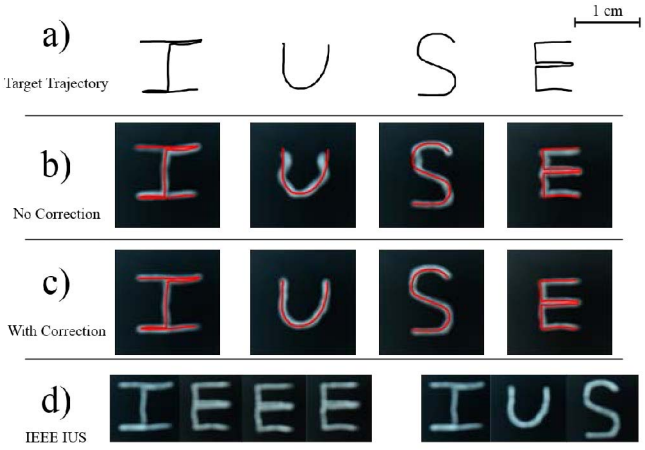

Fig. 8. Application of the correction algorithm on letters trajectory. The position of the target trajectory was normalized against the location of the letter to demonstrate the improvement. a) Target trajectory in the shape of 'I', 'U', 'S' and 'E'. b) Trajectory of the particle without correction. c) Trajectory of the particle with correction. d) Collection of pictures where the particle drew 'IEEE IUS' separately in each instances.

Acknowledgment

T.F. was funded through the Japan Student Services Organization (JASSO) Student Exchange Support Program (Graduate Scholarship for Degree Seeking Students). T.F. acknowledges the support of IEEE UFFC in the form of Student Travel Support.

References

[1] Y. Ochiai, T. Hoshi, and J. Rekimoto, "Pixie dust: graphics generated by levitated and animated objects in computational acoustic-potential field," *ACM Transactions on Graphics (TOG)*, vol. 33, no. 4, p. 85, 2014.

[2] T. Omirou, A. Marzo, S. A. Seah, and S. Subramanian, "Levipath: Modular acoustic levitation for 3d path visualisations," in *Proceedings of the 33rd Annual ACM Conference on Human Factors in Computing Systems*, pp. 309–312, ACM, 2015.

[3] D. R. Sahoo, T. Nakamura, A. Marzo, T. Omirou, M. Asakawa, and S. Subramanian, "JOLED: A Mid-air Display based on Electrostatic Rotation of Levitated Janus Objects," in *Proceedings of the 29th Annual Symposium on User Interface Software and Technology - UIST '16*, (New York, New York, USA), pp. 437–448, ACM Press, 2016.

[4] Y. Uno, H. Qiu, T. Sai, S. Iguchi, Y. Mizutani, T. Hoshi, Y. Kawahara, Y. Kakehi, and M. Takamiya, "Luciola: A Millimeter-Scale Light-Emitting Particle Moving in Mid-Air Based On Acoustic Levitation and Wireless Powering," *Proceedings of the ACM on Interactive, Mobile, Wearable and Ubiquitous Technologies*, vol. 1, pp. 1–17, jan 2018.

[5] M. Prisbrey and B. Raeymaekers, "Ultrasound Noncontact Particle Manipulation of Three-dimensional Dynamic User-specified Patterns of Particles in Air," *Physical Review Applied*, vol. 10, no. 3, p. 034066, 2018.

[6] A. Marzo, T. Corkett, and B. W. Drinkwater, "Ultraino: An Open Phased-Array System for Narrowband Airborne Ultrasound Transmission," *IEEE Transactions on Ultrasonics, Ferroelectrics, and Frequency Control*, vol. 65, no. 1, pp. 102–111, 2018.

[7] L. P. Gor'kov, "On the Forces Acting on a Small Particle in an Acoustical Field in an Ideal Fluid," *Soviet Physics Doklady*, vol. 6, p. 773, 1962.

[8] H. Bruus, "Acoustofluidics 7: The acoustic radiation force on small particles," *Lab on a Chip*, vol. 12, no. 6, p. 1014, 2012.

[9] T. Fushimi, T. L. Hill, A. Marzo, and B. W. Drinkwater, "Nonlinear trapping stiffness of mid-air single-axis acoustic levitators," *Applied Physics Letters*, vol. 113, p. 034102, jul 2018.